Supporting Information

Kodan et al. 10.1073/pnas.1321562111

SI Results

To choose a protein for high-resolution structure determination, we screened the genome of *Cyanidioschyzon merolae* (1), a thermophilic unicellular eukaryote. Our search for the ABC transporter whose amino acid sequence is most similar to that of human P-glycoprotein (hP-gp) resulted in identification of CMD148C (Fig. 1*A*), a half-size ABC transporter whose sequence exhibits 41% and 37% identity to the N-terminal and C-terminal halves of hP-gp, respectively (Fig. S1). We also demonstrated, using a reliable drug-susceptibility assay, that CMD148C functions as a multidrug transporter. Specifically, we expressed CMD148C in *Saccharomyces cerevisiae* strain AD1-8u$^-$, which is susceptible to cytotoxic drugs due to the disruption of seven endogenous ABC transporters (2). Yeast strains expressing CMD148C exhibit resistance to many drugs known to be substrates of hP-gp, such as rhodamine 6G, monensin, etoposide, tetraphenylphosphonium, and fluconazole (Fig. 1*B*). Paclitaxel and vinblastine are well-known substrates of hP-gp (3, 4), but exert little cytotoxicity against yeast cells; therefore, we confirmed and evaluated resistance to these drugs conferred by CMD148C in a drug-susceptibility assay using HEK293 cells (Fig. 1*C* and Fig. S2).

The similarity between CMD148C and hP-gp was underscored by measurements of the ATPase activity of CMD148C in the presence or absence of various substrates of hP-gp (Fig. 1*D*). Most hP-gp substrates stimulated the ATPase activity of purified recombinant CMD148C. The verapamil concentration–dependent ATPase activity exhibited the typical bell-shaped profile observed with hP-gp (5–8) (Fig. 1*E*). Because the substrate specificity and kinetic properties of CMD148C are very similar to those of hP-gp, we referred to this protein as CmABCB1. *C. merolae* is a thermophile; consistent with this, CmABCB1 exhibited much higher thermostability than hP-gp (9) (Fig. S8*E*), suggesting its suitability for high-resolution structural analysis.

SI Materials and Methods

Cloning. For high-resolution structure determination of a eukaryote homolog of human P-gp, the *C. merolae CMD148C* gene (encoding a protein that we named CmABCB1) was cloned by PCR amplification from genomic DNA. For expression of CmABCB1 in *S. cerevisiae* AD1-8u$^-$ (2) cells, the full-length gene was inserted into the multiple cloning site of a pABC3 derivative that includes C-terminal FLAG and His_6 affinity tags (GRDYKDDDDKH_6) (10). The resultant plasmid was transformed into AD1-8u$^-$ cells. For expression of CmABCB1 in *Pichia pastoris* SMD1163 cells, the full-length gene fused to a C-terminal tobacco etch virus (TEV) protease cleavage site, and the His_{10} affinity tag (GSENLYFQGRSH_{10}) was inserted into the multiple cloning site of vector pPICZ-A (Invitrogen Life Technologies). CmABCB1 mutants were generated by site-directed mutagenesis, and sequences were verified before use in transformation of yeasts.

Protein Expression. For crystallization of the WT CmABCB1, large-scale production of the recombinant protein was carried out in *P. pastoris* SMD1163 by fermentative cultivation. A single colony was used to grow a seed culture overnight at 30 °C in 10 mL of yeast extract-peptone-dextrose (YPD) medium with shaking at 240 rpm (BioShaker BR-23FP, TAITEC). The 10-mL seed culture was then inoculated to 1 L of YPD medium, and the culture was grown at 30 °C to an OD_{600} of 5 in a 5-L baffled flask. After being pelleted at 3,000 × *g* for 15 min, the cells were resuspended in 100 mL of Glycerol-complex medium [1% yeast extract, 2% (wt/vol) peptone, 1.34% (wt/vol) yeast nitrogen base, 1.6 μM biotin, and 1% (wt/vol) glycerol]. Using this as the inoculum, fermentative cultivation was performed using a BIOFLO310 fermenter (New Brunswick Scientific) at a 4-L scale. The concentration of dissolved oxygen (DO) was maintained at 40% air saturation by automatically controlling agitation speed (300–800 rpm), ventilation (4–20 L/min) with the air/oxygen mixture, and oxygen content (0–100%) of the mixture. The pH of the fermentation was maintained above 5.0 by supplying a 28% (wt/vol) NH_4OH solution. Polypropylene glycol 2000 was added in 100-μL increments to control excess foaming as necessary. The cells in the fermenter were grown at 30 °C in MGY medium for 10 h. On depletion of the initial glycerol, the glycerol-feed phase was initiated by supplying glycerol and continued for 10 h. To exhaust the remaining glycerol completely, glycerol feeding was stopped for 30 min. After a DO spike was observed, the temperature was dropped from 30 °C to 25 °C, and 8 mL of 100% methanol was added to induce protein expression. Following the 3-h transition phase from glycerol to methanol, the methanol phase was initiated. Cells were harvested 8 h after methanol addition, collected by low-speed centrifugation (3,000 × *g*, 15 min), and stored at −80 °C.

For crystallization of the GAA/VVV mutant CmABCB1 and functional analysis of the WT and mutants, proteins were expressed in *S. cerevisiae* AD1-8u$^-$ cells (2), because large-scale production of these proteins using *P. pastoris* was not necessary. A single colony was used to grow a seed culture overnight at 30 °C in 10 mL of YPD medium with shaking at 240 rpm (BioShaker BR-23FP, TAITEC). The 10-mL seed culture was then inoculated into 1 L of YPD medium in a 5-L baffled flask and grown to an OD_{600} of 0.1; the culture was grown at 25 °C with shaking at 240 rpm using an Innova 4330 incubator shaker (New Brunswick Scientific). After 24 h, cells were harvested by low-speed centrifugation (3,000 × *g*, 15 min) and stored at −80 °C.

Protein Purification. Affinity purification of CmABCB1 was conducted using the C-terminal His_6 or His_{10} affinity tag. Yeast cells were thawed on ice and disrupted using an EmulsiFlex-C4 (Avestin) at 25,000 psi in a buffer containing 20 mM Tris·HCl (pH 7.0) and 150 mM NaCl. The homogenate was clarified by centrifugation at 1,500 × *g* for 15 min to remove the unbroken cells and nuclei, and then crude membranes were collected by ultracentrifugation (100,000 × *g*, 1 h). The membranes were mechanically homogenized and subsequently solubilized for 1 h in binding buffer (20 mM Tris·HCl, pH 7.0, 300 mM NaCl, 20 mM imidazole) containing 1% (wt/vol) $C_{12}E_9$ (Wako). Insoluble material was removed by ultracentrifugation (100,000 × *g*, 1 h), and immobilized metal-ion affinity chromatography (IMAC) resin (Bio-Rad) was added to the supernatant. After a 3-h incubation, the bound protein was eluted with binding buffer containing 300 mM imidazole.

For crystallization of WT CmABCB1, the affinity-purified protein was subjected to protease treatments before size-exclusion chromatography (SEC). The C-terminal His_{10} tag of WT CmABCB1 purified from *P. pastoris* was cleaved off with His-tagged TEV protease, and both the cleaved C-terminal His_{10} tag and TEV protease were removed using an IMAC column. The TEV protease–treated proteins were then subjected to trypsin digestion to remove an additional 92 amino acid residues from the N terminus of CmABCB1; this sequence is not present in other ATP-binding cassette (ABC) transporters, including bacterial ABC exporters (Fig. S1). The N-terminal sequence was required for proper expression; however, removing it increased the monodispersity of the protein in SEC (Fig. S8, *A* and *B*), as well as the protein's crystallizability as judged by X-ray diffraction, but had little effect on the ATPase properties of the purified preparation (Fig. S8, *C* and *D*, and Table S1). Therefore, we used proteolytically N-terminally truncated

CmABCB1 for crystal preparation. The affinity-purified GAA/VVV mutant purified from *S. cerevisiae* was subjected only to trypsin digestion. The trypsin-treated proteins were further purified on an SEC column equilibrated in a buffer composed of 20 mM Tris·HCl (pH 7.0), 150 mM NaCl, and 0.2% (wt/vol) *n*-decyl-β-D-maltopyranoside (βDM; Anatrace), and peak fractions were pooled and concentrated to 10 mg/mL.

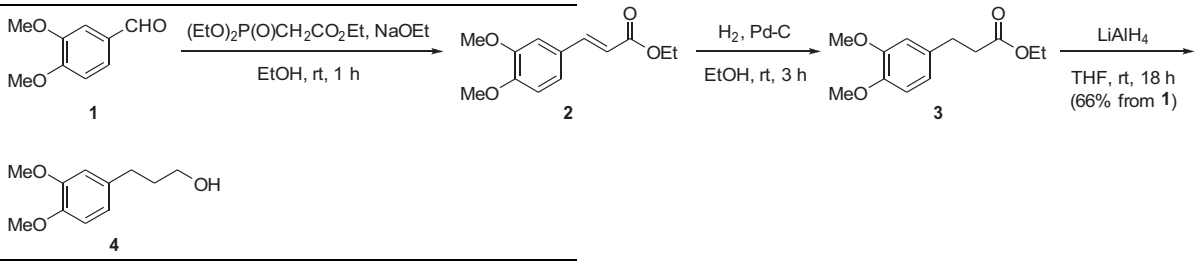

In the preparation used for ATPase activity assays, membranes (5 mg/mL protein) were solubilized using 1% (wt/vol) *n*-dodecyl-β-D-maltopyranoside (βDDM; Anatrace) and purified in 0.05% (wt/vol) βDDM; trypsin and TEV protease treatments were omitted.

Crystallization, Data Collection, and Structure Determination. Co-crystallizations of CmABCB1 with either a newly synthesized verapamil analog (KI-58α) or the tailored cyclic peptide (aCAP, anti-CmABCB1 peptide) were performed by preincubating 0.5 mg/mL CmABCB1 with either 50 μM KI-58α or 10–15 μM aCAP for 16–20 h at 20 °C. Addition of KI-58α improved the diffraction resolution of the crystals. However, in the process of interpretation of the resultant electron density map, no clear electron densities derived from KI-58α were observed. The samples were then concentrated to 10 mg/mL using an Amicon Ultra-4 concentrator unit with a molecular cutoff of 50 kDa (Millipore). The sample was mixed with an equal volume of crystallization solution containing 14–16% (wt/vol) polyethylene glycol 2000 MME and 100 mM magnesium nitrate. Crystals were grown at 20 °C using the sitting-drop vapor-diffusion method. Crystals ($0.2 \times 0.2 \times 0.2$ mm^3) were flash-frozen and stored in liquid nitrogen. Mercury-derivative crystals of CmABCB1 were prepared by soaking the native crystals in reservoir solution supplemented with 1 mM ethyl mercury phosphate (EMP). Diffraction data were collected on beamline BL41XU at SPring-8, using an MX225HE detector.

Initial phases for the CmABCB1 structures were determined by the multiwavelength anomalous dispersion method, using a three-wavelength data set from a mercury derivative. Model building was performed using the COOT (11) and PHENIX (12) packages. Structural refinement was performed in REFMAC5. The quality of the final model was validated with PROCHECK (13) and MolProbity (14). Details of the data collection and refinement statistics are summarized in Tables S2 and S3. Molecular graphics were rendered with PyMOL (15).

Synthesis of *N,N,N*-Tris[4-(3,4-dimethoxyphenyl)butan-1-yl]amine (KI-58α). ***General.*** NMR spectra were obtained on a JEOL JNM-AL300 spectrometer (300 MHz for ^{1}H and 75 MHz for ^{13}C). Chemical shifts are reported in parts per million relative to the internal standards [tetramethylsilane (0.00 ppm) for ^{1}H and $CDCl_3$ (77.0 ppm) for ^{13}C]. High resolution mass spectrometry (HRMS) data was recorded on a JEOL JMS-700 spectrometer. Reagents were used as received from commercial suppliers. Silica gel flash column chromatography was carried out using a Yamazen W-prep 2XY system (Yamazen Corporation) with Hi-Flash columns (silica gel, 40 μm).

3-(3,4-Dimethoxyphenyl)propan-1-ol (4).

To an ethanol solution of sodium ethoxide [prepared from sodium (5.24 g, 228 mmol) and ethanol (250 mL)] was added 3,4-dimethoxybenzaldehyde (**1**; 25.2 g, 152 mmol) and ethyl diethylphosphonoacetate (40.8 g, 182 mmol), and the mixture was stirred for 1 h at room temperature. Ethanol was removed by evaporation, and water (100 mL) was added to the residue. The aqueous layer was extracted with ethyl acetate (100 mL × 3), and the combined organic layer was washed with brine (100 mL), dried over anhydrous magnesium sulfate, and concentrated in vacuo to give ethyl (*E*)-3-(3,4-dimethoxyphenyl)acrylate (**2**; 44.1 g) as a pale yellow solid. ^{1}H NMR (300 MHz, $CDCl_3$) δ 1.34 (3H, t, J = 7.2 Hz), 3.91 (6H, s), 4.26 (2H, q, J = 7.2 Hz), 6.31 (1H, d, J = 16.1 Hz), 6.86 (1H, d, J = 8.4 Hz), 7.05 (1H, d, J = 2.1 Hz), 7.10 (1H, dd, J = 8.4 and 2.1 Hz), 7.63 (1H, d, J = 16.1 Hz).

The crude material (**2**; 44.1 g) was dissolved in ethanol (100 mL), and to the solution was added 10% (wt/wt) palladium carbon (4.41 g). Hydrogen gas was bubbled into the mixture for 3 h at room temperature. The catalyst was filtered off, and the filtrate was concentrated in vacuo to give ethyl 3-(3,4-dimethoxyphenyl)propanoate (**3**; 34.8 g) as a pale yellow oil. ^{1}H NMR (300 MHz, $CDCl_3$) δ 1.24 (3H, t, J = 7.2 Hz), 2.60 (2H, t, J = 7.8 Hz), 2.90 (2H, t, J = 7.8 Hz), 3.85 (3H, s), 3.87 (3H, s), 4.13 (2H, q, J = 7.2 Hz), 6.73–6.76 (2H, m), 6.80 (1H, d, J = 8.4 Hz).

The crude material (**3**; 34.8 g) was dissolved in anhydrous tetrahydrofuran (500 mL), and the solution was cooled in an ice bath. To the solution was added lithium aluminum hydride (11.1 g, 292 mmol) in small portions, and the mixture was stirred for 18 h at room temperature. To the reaction mixture was successively added water (11.1 mL) and 10% (wt/vol) aqueous sodium hydroxide solution (11.1 mL), dropwise at 0 °C. Additional water (33.3 mL) was added, and the mixture was dried over anhydrous magnesium sulfate. The insoluble materials were filtered off, and the filtrate was concentrated in vacuo to give compound **4** (19.5 g, 66% from **1**) as a colorless oil. This product was used without purification. ^{1}H NMR (300 MHz, $CDCl_3$) δ 1.67 (1H, br, s), 1.85–1.90 (2H, m), 2.66 (2H, dd, J = 8.1 and 7.5 Hz), 3.64–3.70 (2H, m), 3.85 (3H, s), 3.87 (3H, s), 6.72–6.75 (2H, m), 6.80 (1H, d, J = 8.4 Hz).

4-(3,4-Dimethoxyphenyl)butanenitrile (6).

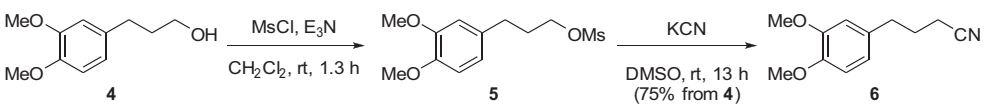

To an ice-cold solution of 3-(3,4-dimethoxyphenyl)propan-1-ol (**4**; 24.1 g, 123 mmol) and triethylamine (25.9 mL, 186 mmol) in dichloromethane (200 mL) was added methanesulfonyl chloride (10.6 mL, 137 mmol) dropwise, and the mixture was stirred for 1.3 h at room temperature. Water (100 mL) was added to the reaction mixture, and the separated aqueous layer was extracted with dichloromethane (75 mL × 3). The combined organic layer was washed with saturated aqueous sodium hydrogen carbonate solution (75 mL), dried over anhydrous magnesium sulfate, and concentrated in vacuo to give 3-(3,4-dimethoxyphenyl)propan-1-yl methanesulfonate (**5**; 34.0 g) as a red oil. ^{1}H NMR (300 MHz, $CDCl_3$) δ 2.06 (2H, tt, J = 7.5 and 6.2 Hz), 2.70 (2H, t, J = 7.5 Hz), 3.00 (3H, s), 3.86 (3H, s), 3.88 (3H, s), 4.23 (2H, t, J = 6.2 Hz), 6.72–6.74 (2H, m), 6.81 (1H, d, J = 8.7 Hz).

The crude material (**5**; 34.0 g) was dissolved in anhydrous dimethyl sulfoxide (150 mL), and powdered sodium cyanide (16.1 g, 247 mmol) was added to the solution. After stirring for 13 h at room temperature, saturated aqueous solution of sodium hydrogen carbonate (150 mL) was added to the mixture. The aqueous layer was extracted with toluene (100 mL × 3), and the combined organic layer was washed with brine (100 mL), dried over anhydrous magnesium sulfate, and concentrated in vacuo. The residue was purified by silica gel flash column chromatography (hexane:ethyl acetate = 75:25) to give compound **6** (19.0 g, 75% from **4**) as a yellow oil. ^{1}H NMR (300 MHz, $CDCl_3$) δ 1.96 (2H, tt, J = 7.2 and 7.2 Hz), 2.32 (2H, t, J = 7.2 Hz), 2.73 (2H, t, J = 7.2 Hz), 3.87 (3H, s), 3.88 (3H, s), 6.71–6.74 (2H, m), 6.81 (1H, d, J = 8.1 Hz).

[4-(3,4-Dimethoxyphenyl)butan-1-yl]amine (7).

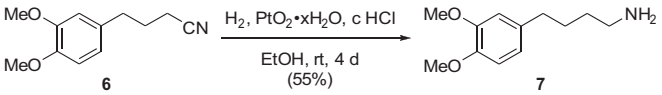

Hydrogen gas was bubbled into a mixture of 4-(3,4-dimethoxyphenyl)butanenitrile (**6**; 10.0 g, 48.7 mmol), ethanol (100 mL), concentrated hydrochloric acid (10 mL), and platinum oxide hydrate (200 mg) for 4 d at room temperature. The catalyst was filtered off, and the filtrate was made basic by the addition of 10% (wt/vol) aqueous sodium hydroxide solution. The mixture was concentrated, and water (50 mL) was added to the residue. The aqueous layer was extracted with chloroform (50 mL × 3), and the combined organic layer was washed with 10% (wt/vol) aqueous sodium hydroxide solution (50 mL), dried over anhydrous magnesium sulfate, and concentrated in vacuo. The residue was purified by silica gel flash column chromatography [ethyl acetate, then chloroform:methanol = 90:10, both solvent systems contained 1% (vol/vol) triethylamine] to give compound **7** (5.58 g, 55%) as a yellow oil. ^{1}H NMR (300 MHz, $CDCl_3$) δ 1.44–1.54 (2H, m), 1.49 (2H, br s), 1.59–1.69 (2H, m), 2.58 (2H, t, J = 7.7 Hz), 2.72 (2H, t, J = 6.8 Hz), 3.86 (3H, s), 3.88 (3H, s), 6.71–6.73 (2H, m), 6.79 (1H, d, J = 8.4 Hz).

4-(3,4-Dimethoxyphenyl)butanal (8).

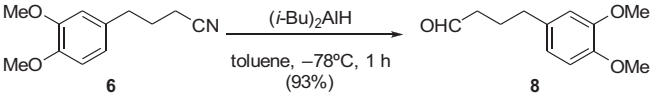

To a solution of 4-(3,4-dimethoxyphenyl)butanenitrile (**6**; 17.0 g, 82.8 mmol) in anhydrous toluene (150 mL) was added diisobutylaluminum hydride solution (1.0 M in toluene, 99 mL, 99.0 mmol) dropwise at −78 °C under argon atmosphere. The reaction mixture was stirred for 1 h at the same temperature, and methanol (30 mL) was added dropwise to the solution. The mixture was allowed to warm up to room temperature, and diethyl ether (150 mL) and 1 N HCl (150 mL) were added. After stirring for 30 min at room temperature, the separated aqueous layer was extracted with diethyl ether (75 mL × 3). The combined organic layer was washed with saturated aqueous sodium hydrogen carbonate solution (75 mL), dried over anhydrous magnesium sulfate, and concentrated in vacuo to give compound **8** (16.0 g, 93%) as a yellow oil. This product was used without purification. ^{1}H NMR (300 MHz, $CDCl_3$) δ 1.95 (2H, tt, J = 7.5 and 7.5 Hz), 2.46 (2H, td, J = 7.5 and 1.5 Hz), 2.61 (2H, t, J = 7.5 Hz), 3.86 (3H, s), 3.87 (3H, s), 6.70–6.73 (2H, m), 6.80 (1H, d, J = 8.4 Hz), 9.76 (1H, t, J = 1.5 Hz).

N,N,N-*Tris[4-(3,4-dimethoxyphenyl)butan-1-yl]amine (9)* and N,N-*bis[4-(3,4-dimethoxyphenyl)butan-1-yl]amine (10).*

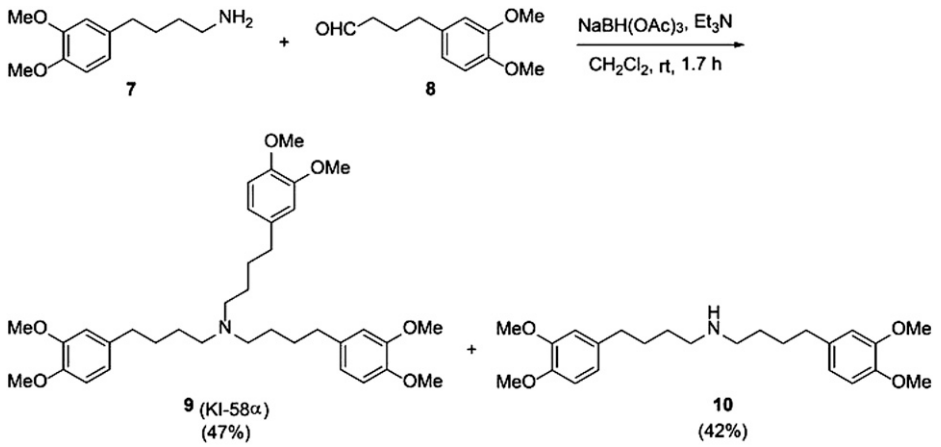

To a solution of compound **8** (3.58 g, 17.2 mmol) and triethylamine (3.1 mL, 22.2 mmol) in dichloromethane (100 mL) was added compound **7** (5.75 g, 27.5 mmol), and the mixture was stirred for 5 min at room temperature. Sodium triacetoxyborohydride (5.82 g, 27.5 mmol) was added, and the mixture was stirred for 1.7 h at room temperature. Aqueous solution of saturated sodium hydrogen carbonate (100 mL) was added to the reaction mixture, and the separated organic layer was extracted with dichloromethane (50 mL × 3). The combined organic layer was washed with brine (50 mL), dried over anhydrous magnesium sulfate, and concentrated in vacuo. The

residue was purified by silica gel flash column chromatography [chloroform:methanol = 95:5, containing 1% (vol/vol) triethylamine] to give compound **9** (2.40 g, 47%) as a yellow oil. ^{1}H NMR (300 MHz, $CDCl_3$) δ 1.41–1.64 (12H, m), 2.40 (6H, t, J = 7.2 Hz), 2.56 (6H, t, J = 7.5 Hz), 3.85 (9H, s), 3.86 (9H, s), 6.69–6.79 (9H, m). ^{13}C NMR (75 MHz, $CDCl_3$) δ 26.8 (3C), 29.6 (3C), 35.4 (3C), 53.9 (3C), 55.7 (3C), 55.8 (3C), 111.1 (3C), 111.7 (3C), 120.1 (3C), 135.3 (3C), 147.0 (3C), 148.7 (3C). HRMS-FAB (*m*/*z*): $[M + H]^+$ calculated for $C_{36}H_{52}NO_6$, 594.3795; found, 594.3777. Compound **10** (2.92 g, 42%) was also obtained as a yellow oil. ^{1}H NMR (300 MHz, $CDCl_3$) δ 1.47–1.68 (8H, m), 2.57 (4H, t, J = 7.4 Hz), 2.61 (4H, t, J = 7.4 Hz), 3.85 (6H, s), 3.87 (6H, s), 6.70–6.80 (6H, m). ^{13}CNMR (75 MHz, $CDCl_3$) δ 29.4 (2C), 29.8 (2C), 35.4 (2C), 49.9 (2C), 55.7 (2C), 55.8 (2C), 111.1 (2C), 111.6 (2C), 120.1 (2C), 135.1 (2C), 147.0 (2C), 148.7 (2C). HRMS-FAB (*m*/*z*): $[M + H]^+$ calcd for $C_{24}H_{36}NO_4$, 402.2644; found, 402.2637.

Selection and Chemical Synthesis of a CmABCB1-Binding Cyclic Peptide (aCAP). The selection was performed using an NNK (N=A/C/G/T, K=G/T) library according to literature protocol with modifications (16).

Initiator $tRNA^{fMet}_{CAU}$ was charged by flexizyme using chemically activated *N*-chloroacetyl-D-tryptophan as previously described (17). For the first round of the selection, His-tagged CmABCB1 (75 pmol) was used to saturate the His-tag binding sites on prewashed Invitrogen Dynabeads His-Tag Isolation and Pulldown magnetic beads (120 μg) in CmABCB1 storage buffer [20 mM Tris·HCl, 150 mM NaCl, 0.02% (wt/vol) n-decyl-β-maltoside, pH 7.0, 165 μL]. SDS/PAGE analysis revealed that 120 μg of magnetic beads bound 37.5 pmol His-tagged CmABCB1. For all subsequent rounds, His-tagged CmABCB1 (25 pmol) was used to saturate the His-tag binding sites on Invitrogen Dynabeads His-Tag Isolation and Pulldown magnetic beads (40 μg) in CmABCB1 storage buffer (10 μL). The peptide library for the first round of selection was produced using 200 pmol of mRNA-puromycin conjugate and 5.25 nmol of ClAc-D-Trp-$tRNA^{fMet}_{CAU}$ in a translation reaction mixture with a volume of 150 μL (16). 2× Blocking solution [20 mM Tris·HCl, 150 mM NaCl, 0.02% (wt/vol) n-decyl-β-maltoside, 0.2% (wt/vol) acetylated BSA, pH 7.0; 165 μL] was added to each of the desalted peptide-mRNA solutions.

After desalting the mRNA-cyclic peptide conjugates from round 2 and subsequent rounds, nonspecific bead-binding cyclic peptides were removed by incubating the desalted cyclic peptide–mRNA conjugates with 200-μg magnetic beads for 30 min at 4 °C. The supernatant was subjected to four additional preclearances using 100 μg of magnetic bead at 4 °C for 30 min each. For round 6, only 10% of the prepared peptide–mRNA molecules were applied to the CmABCB1 binding step to avoid saturation. The cDNA obtained after round 6 was ligated into the plasmid pGEM-T Easy by TA-cloning. DNA sequences were confirmed by FASMAC Co. Ltd.

The binding abilities of clones #6-1, #6-2, #6-3, and #6-5 (aCAP) were determined using single-clone display. The assay conditions used were the same conditions as the second round of selection. The selected cyclic peptides were chemically synthesized with only a single glycine-carboxamide in place of the $(Gly\text{-}Ser)_3$ linker used in the selection. All cyclic peptides were synthesized using an automated peptide synthesizer (Syro; Biotage) as previously described (16). Following synthesis, peptides were cleaved from the resin and cyclized. Cyclic peptides were purified using HPLC (Imtakt Cadenza CD-C18 250 × 10-mm column; Gilson HPLC). The mass was verified by MALDI-TOF MS (Autoflex II; Bruker Daltronics).

i) MALDI-TOF: calculated for $C_{81}H_{116}N_{21}O_{18}S^+$ (#6-1): 1702.852; observed: 1703.402

ii) MALDI-TOF: calculated for $C_{103}H_{152}N_{23}O_{27}S^+$ (#6-2): 2175.094; observed: 2175.591

iii) MALDI-TOF: calculated for $C_{109}H_{155}N_{22}O_{27}S^+$ (#6-3): 2236.115; observed: 2236.750

iv) MALDI-TOF: calculated for $C_{100}H_{140}N_{25}O_{25}S^+$ (#6-5): 2123.017; observed: 2123.580

Compound #6-5 exhibited the highest affinity to CmABCB1 in the ATPase inhibition assay, and this is the compound referred to as aCAP (anti-CmABCB1 peptide).

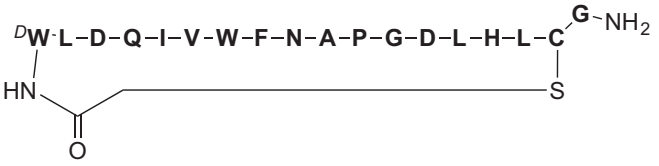

Drug-Susceptibility Assays in Yeast. *S. cerevisiae* AD1-8u$^-$ expressing WT or mutant CmABCB1 were precultured in YPD medium at 30 °C for 16 h, inoculated in YPD medium to an OD_{600} of 0.5, and then cultured at 30 °C to an OD_{600} of 2–3. These cultures were then diluted in YPD medium to an OD_{600} of 0.2, and 50 μL of each cell suspension was inoculated into 450 μL YPD medium containing a drug at the indicated concentration in a 96-well V-shaped MasterBlock (Greiner Bio One). After culture at 30 °C for 13–14 h, OD_{600} values of the cell suspensions were measured. For each mutant, the assay was performed using four to eight clones, and the averages and SDs of the measured values were calculated. Glu610 is the catalytic residue, corresponding to Glu556 or Glu1201 in hP-gp (18), and the Ala substitution of the residue abolished the transporter function (Fig. S6*A*). The expression levels of mutant proteins were evaluated by Western blot analysis to detect the FLAG tag fused to the C terminus of CmABCB1. Total cellular protein (20 μg) from AD1-8u$^-$ cells was separated on an SDS polyacrylamide gel and electroblotted onto a nitrocellulose membrane. Proteins were detected by Western blot analysis using mouse monoclonal anti-FLAG antibody (diluted 1:4,000) or mouse monoclonal anti-GAPDH antibody (diluted 1:4,000). Expression levels of the mutants were approximately equal to that of WT (Fig. S6*B*).

Transport Activity Assays and Cellular Localization Analysis in HEK293 Cells. For cell viability assays in mammalian cells, the cDNA encoding CmABCB1 that includes C-terminal FLAG and His_6 affinity tags ($GRDYKDDDDKH_6$) was subcloned into the pIRES-hyg3 vector. The resultant plasmid was transfected into HEK293 cells, and a population of stably transfected cells was selected by the addition of 0.35 mg/mL hygromycin. To obtain highly expressing cells, cells were further selected in 20 nM vinblastine for 1 wk. Mock-transfected and CmABCB1-expressing HEK293 cells were seeded at a cell density of 1,000 cells per well. Cells were incubated for 3 d after addition of drugs, and cell viability was measured by the 3-(4,5-dimethylthiazol-2-yl)-2,5-diphenyl tetrazolium bromide (MTT) assay (19) with slight modifications. In brief, cells were incubated with DMEM containing 0.1 mg/mL MTT for more than 3 h, and the generated formazan dye was dissolved in DMSO and quantified by measuring the absorption at 560 nm. For the calcein-AM transport assay, mock-transfected and CmABCB1-expressing HEK293 cells were incubated with 50 nM of calcein-AM for 30 min in the presence or absence of 50 μM verapamil and cellular accumulation of calcein was estimated by flow cytometry (excitation: 488 nm/emission: 533 nm). Cellular localization was analyzed by immunostaining and confocal microscopy. Cells stably expressing CmABCB1 were fixed with cold methanol. For blocking, fixed cells were incubated with 10% (vol/vol) goat serum in PBS^+ (PBS containing 0.1 g/L of $CaCl_2$ and $MgCl_26H_2O$). Cells were incubated for 1 h

with rabbit polyclonal anti-FLAG antibody (SIGMA) diluted 1:1,000 in PBS^+ containing 10% (vol/vol) goat serum, and then incubated with fluorescent Alexa488-conjugated anti-rabbit IgG (Molecular Probes) for 1 h. Cells were viewed with a 63× Plan-Neofluar oil immersion objective using a Zeiss confocal microscope (LSM5 Pascal). No expression of endogenous *MDR1* in HEK293/CmABCB1 was confirmed by RT-PCR.

ATPase Measurements. ATPase activity was measured in 50 mM Tris·HCl (pH 7.5), 150 mM NaCl, 0.1 mM EGTA, 0.05% (wt/vol) βDDM, and 10 mM $MgCl_2$, with or without ATP and/or compounds, at 37 °C. The amount of inorganic phosphate released from ATP was measured using a colorimetric method (20). The initial hydrolysis rate was calculated by plotting the amount of inorganic phosphate as a function of reaction time.

Determination of Kinetic Parameters for the ATPase Reaction. Four different analyses were performed. For ATP, kinetic parameters were determined using the Michaelis-Menten equation (Eq. **S1**)

$$v = \frac{k_{cat}[e][s]}{K_m^{ATP} + [s]}. \qquad \textbf{[S1]}$$

For rhodamine 6G, verapamil, or aCAP, parameters were determined using the following equations (Eqs. **S2–S4**) (7, 8):

$$v = [e]\left(k_{basal} + \frac{(k_{sub} - k_{basal})[s]}{K_m^{Drug} + [s]}\right)\left(1 - \frac{[s]}{K_i^{Drug} + [s]}\right), \qquad \textbf{[S2]}$$

$$v = [e]\left(k_{basal} + \frac{(k_{sub} - k_{basal})[s]}{K_m^{Drug} + [s]}\right), \qquad \textbf{[S3]}$$

$$v = [e]\left(\frac{k_{basal} - k_{sub}}{1 + \frac{[s]}{K_i}} + k_{sub}\right), \qquad \textbf{[S4]}$$

where v is the initial ATP hydrolysis rate, $[e]$ is the CmABCB1 concentration, $[s]$ is the substrate concentration, k_{basal} is the catalytic rate constant of basal ATPase activity in the absence of drug, k_{sub} is the catalytic rate constant of drug-dependent ATPase activity, K_m^{ATP} is the apparent Michaelis constant for ATP in the absence of transport substrates, K_m^{Drug} is the Michaelis constant for transport substrates (rhodamine 6G or verapamil) with 5 mM ATP, K_i^{Drug} is the inhibition constant for substrate inhibition by transport substrates, and K_i is the apparent inhibition constant for rhodamine 6G or aCAP. Fitting was carried out using GRAFIT (Erithacus Software).

1. Matsuzaki M, et al. (2004) Genome sequence of the ultrasmall unicellular red alga Cyanidioschyzon merolae 10D. *Nature* 428(6983):653–657.
2. Nakamura K, et al. (2001) Functional expression of Candida albicans drug efflux pump Cdr1p in a Saccharomyces cerevisiae strain deficient in membrane transporters. *Antimicrob Agents Chemother* 45(12):3366–3374.
3. Greenberger LM, Lothstein L, Williams SS, Horwitz SB (1988) Distinct P-glycoprotein precursors are overproduced in independently isolated drug-resistant cell lines. *Proc Natl Acad Sci USA* 85(11):3762–3766.
4. Ueda K, Cardarelli C, Gottesman MM, Pastan I (1987) Expression of a full-length cDNA for the human "MDR1" gene confers resistance to colchicine, doxorubicin, and vinblastine. *Proc Natl Acad Sci USA* 84(9):3004–3008.
5. Doige CA, Yu X, Sharom FJ (1992) ATPase activity of partially purified P-glycoprotein from multidrug-resistant Chinese hamster ovary cells. *Biochim Biophys Acta* 1109(2):149–160.
6. Litman T, Zeuthen T, Skovsgaard T, Stein WD (1997) Competitive, non-competitive and cooperative interactions between substrates of P-glycoprotein as measured by its ATPase activity. *Biochim Biophys Acta* 1361(2):169–176.
7. Al-Shawi MK, Polar MK, Omote H, Figler RA (2003) Transition state analysis of the coupling of drug transport to ATP hydrolysis by P-glycoprotein. *J Biol Chem* 278(52): 52629–52640.
8. Sato T, et al. (2009) Functional role of the linker region in purified human P-glycoprotein. *FEBS J* 276(13):3504–3516.
9. Kodan A, et al. (2009) Improved expression and purification of human multidrug resistance protein MDR1 from baculovirus-infected insect cells. *Protein Expr Purif* 66(1):7–14.
10. Lamping E, et al. (2007) Characterization of three classes of membrane proteins involved in fungal azole resistance by functional hyperexpression in Saccharomyces cerevisiae. *Eukaryot Cell* 6(7):1150–1165.
11. Emsley P, Cowtan K (2004) Coot: Model-building tools for molecular graphics. *Acta Crystallogr D Biol Crystallogr* 60(Pt 12 Pt 1):2126–2132.
12. Adams PD, et al. (2002) PHENIX: Building new software for automated crystallographic structure determination. *Acta Crystallogr D Biol Crystallogr* 58(Pt 11):1948–1954.
13. Laskowski RA, MacArthur MW, Moss DS, Thornton JM (1993) PROCHECK: A program to check the stereochemical quality of protein structures. *J Appl Cryst* 26(2):283–291.
14. Davis IW, et al. (2007) MolProbity: All-atom contacts and structure validation for proteins and nucleic acids. *Nucleic Acids Res* 35(Web Server issue):W375–W383.
15. Schrödinger L (2010) *The PyMOL Molecular Graphics System, Version 1.6* (Schrödinger, LLC, New York).
16. Hipolito CJ, Tanaka Y, Katoh T, Nureki O, Suga H (2013) A macrocyclic peptide that serves as a cocrystallization ligand and inhibits the function of a MATE family transporter. *Molecules* 18(9):10514–10530.
17. Yamagishi Y, et al. (2011) Natural product-like macrocyclic N-methyl-peptide inhibitors against a ubiquitin ligase uncovered from a ribosome-expressed de novo library. *Chem Biol* 18(12):1562–1570.
18. Sauna ZE, Müller M, Peng XH, Ambudkar SV (2002) Importance of the conserved Walker B glutamate residues, 556 and 1201, for the completion of the catalytic cycle of ATP hydrolysis by human P-glycoprotein (ABCB1). *Biochemistry* 41(47): 13989–14000.
19. Mosmann T (1983) Rapid colorimetric assay for cellular growth and survival: Application to proliferation and cytotoxicity assays. *J Immunol Methods* 65(1-2):55–63.
20. Chifflet S, Torriglia A, Chiesa R, Tolosa S (1988) A method for the determination of inorganic phosphate in the presence of labile organic phosphate and high concentrations of protein: Application to lens ATPases. *Anal Biochem* 168(1):1–4.

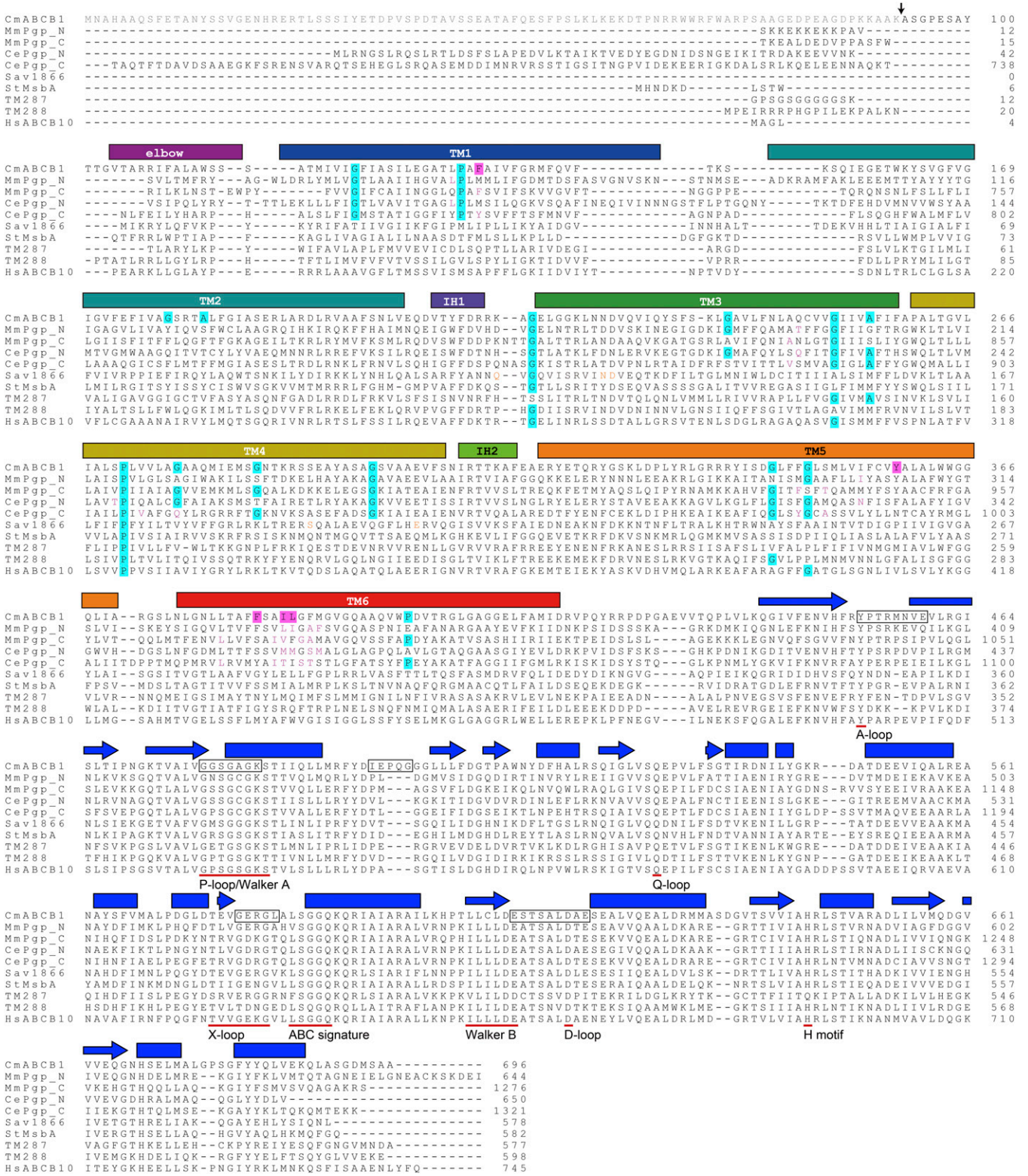

Fig. S1. Amino acid sequence alignment of ABC exporters whose structures have been determined. *C. merolae* ABCB1 (CmABCB1) is aligned with the N- and C-terminal halves of *M. musculus* P-gp (GI, 153791547), the N- and C-terminal halves of *C. elegans* P-gp (GI, 17541710), *S. aureus* Sav1866 (GI, 15924856), *S. typhimurium* MsbA (GI, 16759854), *T. maritima* TM287 (GI, 15643056) and TM288 (GI, 15643057), and *H. sapiens* ABCB10 (GI, 171184400). Secondary-structure elements of CmABCB1 are indicated above the sequences. The flexible N-terminal sequences removed by trypsin digestion are shown in gray letters. The trypsin cleavage site is indicated by a black arrow. Residues important for the interaction with rhodamine 6G are highlighted in pink. Residues that form a Gly zipper or act as a hinge for each TM are highlighted in cyan. Residues forming hydrogen bonds between TM3 and TM4 in Sav1866 are shown in orange letters. Residues reported in previous studies (1–3) to be important for interactions with drugs are shown in magenta. The regions in which the nucleotide-binding domains (NBDs) of CmABCB1 and the Sav1866 structures do not conform in the superposition (Fig. S7*A*) are indicated by boxes. The alignment was performed using PROMALS3D with manual adjustment.

1. Loo TW, Bartlett MC, Clarke DM (2006) Transmembrane segment 1 of human P-glycoprotein contributes to the drug-binding pocket. *Biochem J* 396(3):537–545.
2. Loo TW, Bartlett MC, Clarke DM (2006) Transmembrane segment 7 of human P-glycoprotein forms part of the drug-binding pocket. *Biochem J* 399(2):351–359.
3. Loo TW, Clarke DM (2005) Do drug substrates enter the common drug-binding pocket of P-glycoprotein through "gates"? *Biochem Biophys Res Commun* 329(2):419–422.

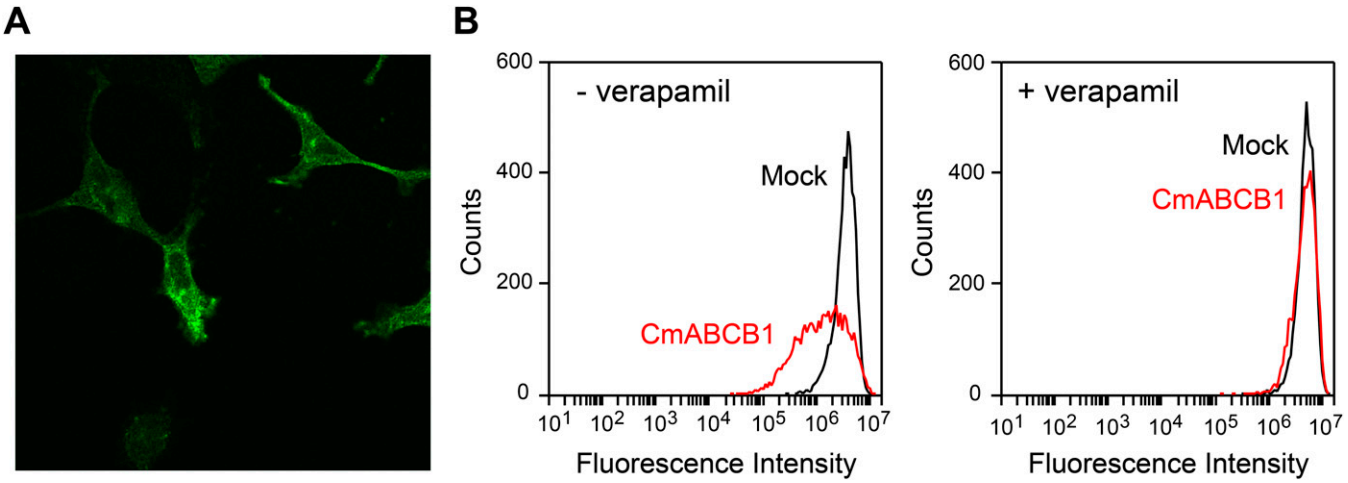

Fig. S2. Cellular localization and calcein-AM export activity of CmABCB1 in HEK293 cells. (*A*) Cellular localization of CmABCB1 in HEK293 cells. Cells were fixed with methanol and CmABCB1 was visualized with rabbit polyclonal anti FLAG antibody. CmABCB1 localized at the cell surface and the intracellular compartment. (*B*) Calcein-AM efflux assay. Cells expressing CmABCB1 (red) and mock-transfected (black) cells were incubated with calcein-AM in the presence or absence of 50 μM verapamil and accumulated calcein was quantified with flow cytometry. The accumulation of calcein was reduced in CmABCB1-expressing cells, and the prevention of calcein accumulation was completely abolished by the addition of verapamil.

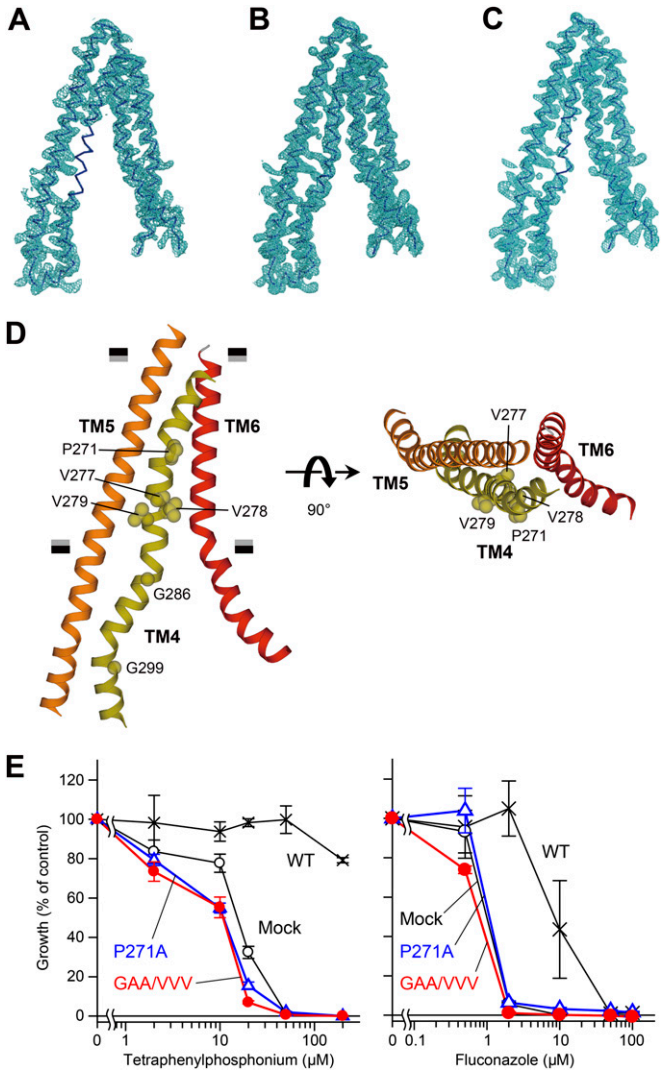

Fig. S3. The G277V/A278V/A279V mutation. (*A*–*C*) TM4 electron density of an initial model of WT CmABCB1 (*A*), a refined model of GAA/VVV (*B*), and a refined model of WT CmABCB1, referenced to the refined model of GAA/VVV (*C*). Shown in blue mesh is a $2F_{obs}–F_{calc}$ electron-density map contoured at 1.0σ. The Cα trace is superimposed on the electron-density map of TM3, TM4, TM5, and TM6. (*D*) Ribbon diagrams of TM4, TM5, and TM6 of CmABCB1 (GAA/VVV mutant), viewed parallel (*Left*) and perpendicular (*Right*) to the plane of the membrane. Horizontal black bars represent the expected positions of the hydrophilic surfaces of the lipid membrane; gray bars represent the expected positions of the hydrophobic surfaces. (*E*) Tetraphenylphosphonium bromide and fluconazole susceptibilities of yeast cells expressing TM4 mutants GAA/VVV and P271A. AD1-8u$^-$ cells expressing WT CmABCB1 (black cross), GAA/VVV (red closed circle), and P271A (blue open triangles) mutants were grown in various concentrations of drugs. For each drug assayed, mock-transfected AD1-8u$^-$ cells (open circles) were also grown as controls. Data are means ± SD (n = 4).

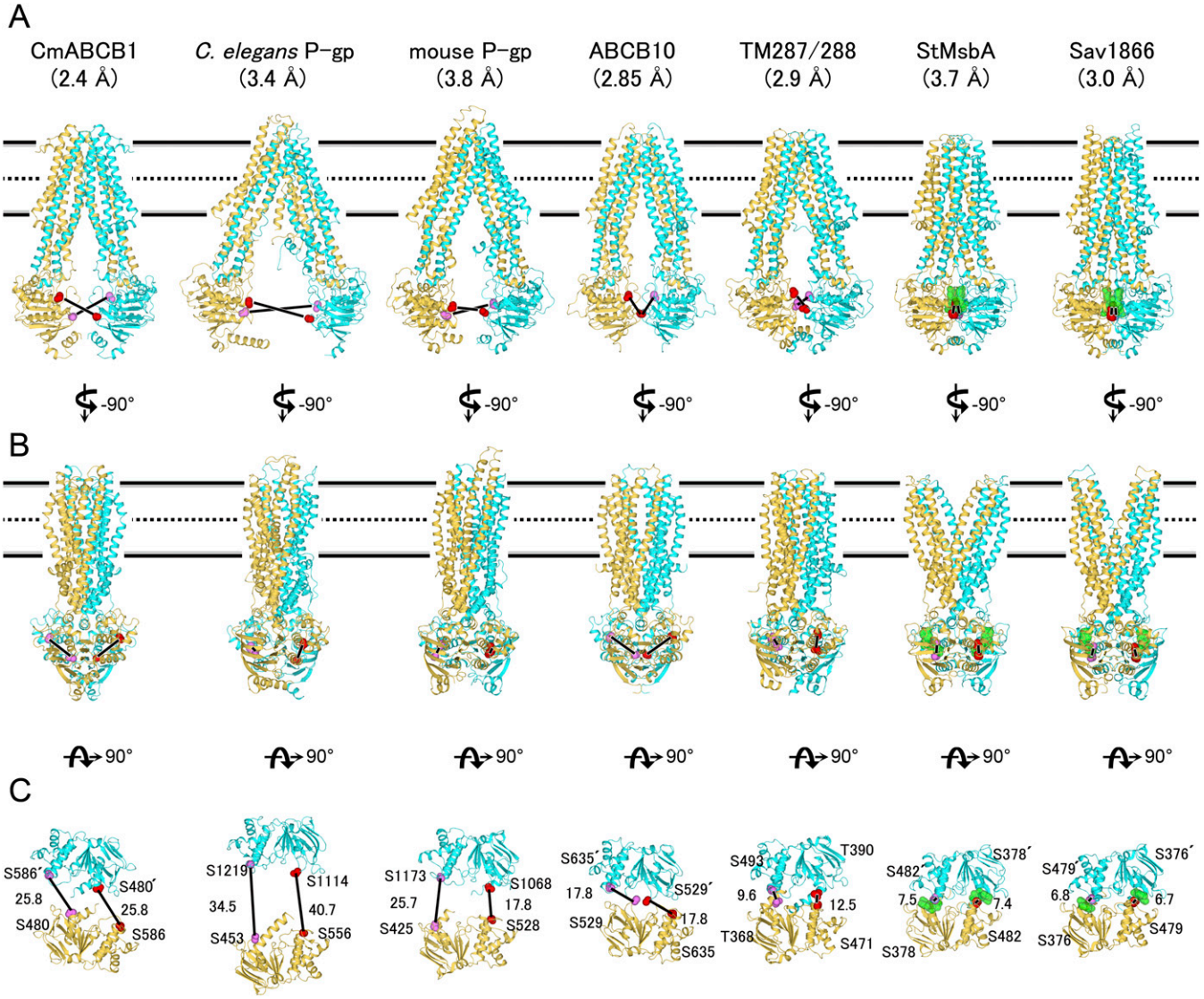

Fig. S4. Comparison of the structure of CmABCB1 with published structures of ABC transporters. Shown is alignment of overall structures (*A* and *B*) and NBDs (*C*) of CmABCB1 (PDB code 3WMG), *C. elegans* P-gp (PDB code 4F4C), mouse P-gp (PDB code 4M1M) (1), ABCB10 (PDB code 4AYT) (2), TM287/288 (PDB code 3QF4), StMsbA (PDB code 3B60), and Sav1866 (PDB code 2HYD), viewed parallel to the plane of the membrane (*A* and *B*) and from the extracellular side (*C*). The resolutions of each crystal structure are indicated in parentheses. The distances (Å) between the Cα atom of the first Ser (Ser480 in CmABCB1; Thr368/Thr390 in TM287/288) in the P-loop/WalkerA motif and that of the Ser (Ser586 in CmABCB1) in the ABC signature motif of the adjacent NBD are indicated by bold numbers with the black lines. These Ser or Thr residues are shown as red spheres. The nucleotides bound to StMsbA and Sav1866 are shown as green spheres. Horizontal black bars represent the expected positions of the hydrophilic surfaces of the lipid membrane; gray bars represent the expected positions of the hydrophobic surfaces. Thick dashed lines represent the middle of the membrane bilayer.

1. Li J, Jaimes KF, Aller SG (2014) Refined structures of mouse P-glycoprotein. *Protein Sci* 23(1):34–46.
2. Shintre CA, et al. (2013) Structures of ABCB10, a human ATP-binding cassette transporter in apo- and nucleotide-bound states. *Proc Natl Acad Sci USA* 110(24):9710–9715.

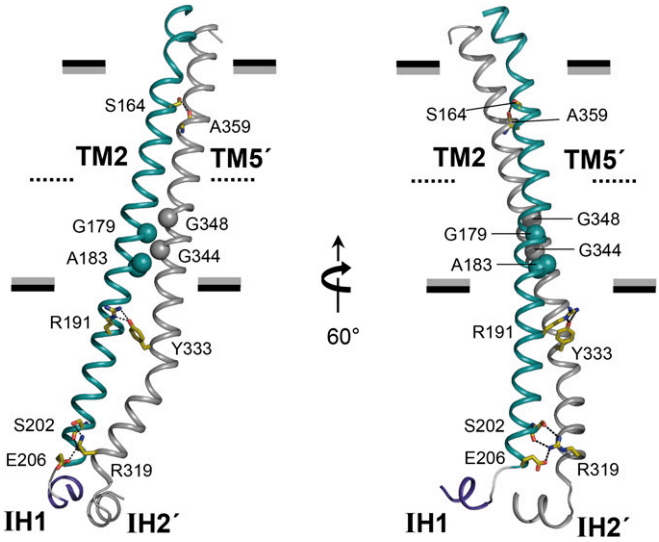

Fig. S5. TM2–TM5′ interaction. Residues acting as Gly-zipper motifs are shown as spheres, and residues forming hydrogen bonds are shown as sticks. Horizontal black bars represent the expected positions of the hydrophilic surfaces of the lipid membrane; gray bars represent the expected positions of the hydrophobic surfaces.

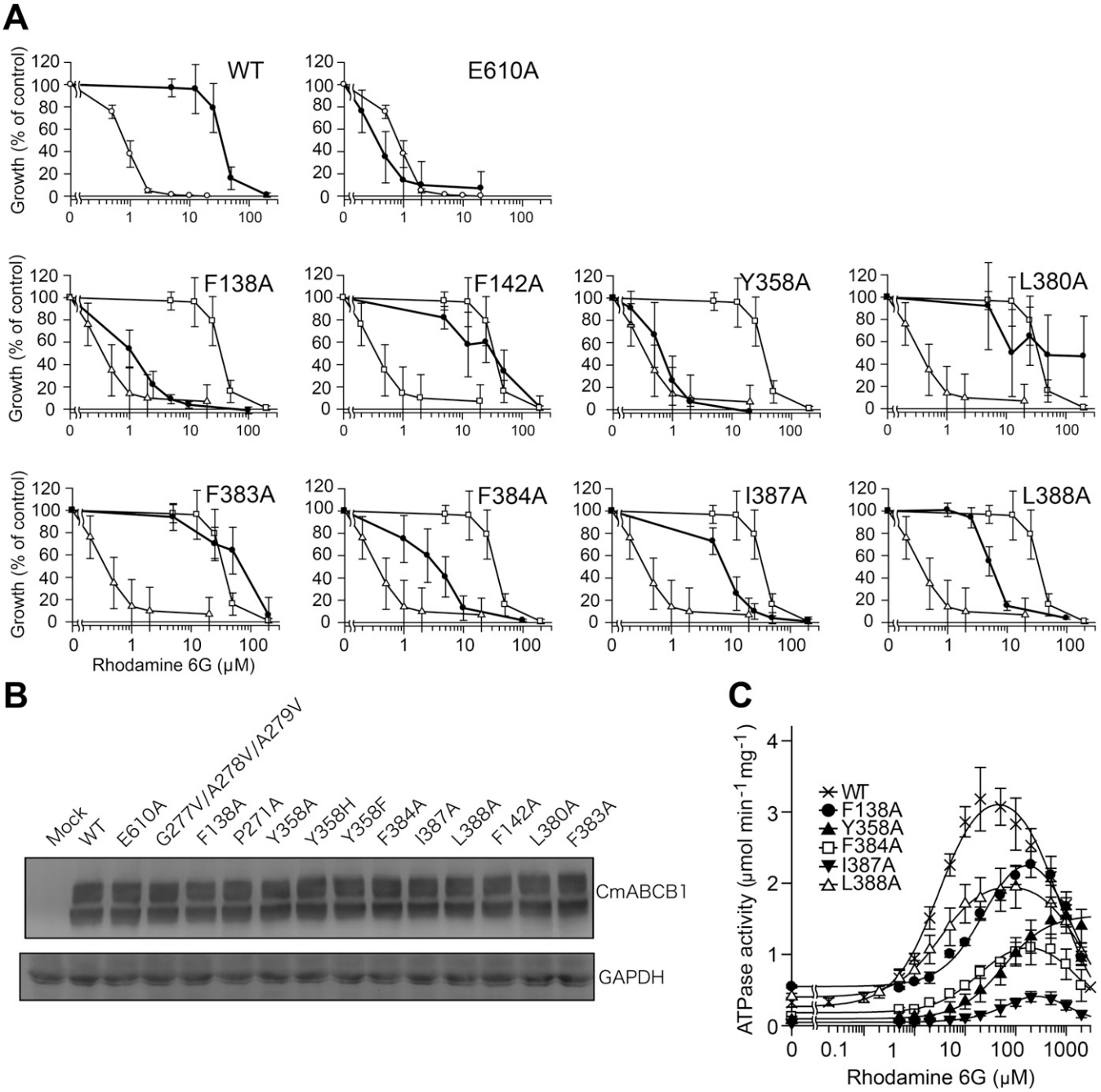

Fig. S6. Analysis of functional residues of CmABCB1. (*A*) Rhodamine 6G susceptibility of yeast cells expressing CmABCB1 mutants. Yeast cells expressing WT CmABCB1 or mutant proteins were cultured with various concentrations of rhodamine 6G. Cell proliferation was analyzed by measuring the absorbance at 600 nm, and growth (% of control) was plotted against rhodamine 6G concentration (filled circles with thick lines). In the graphs of the WT and an ATPase-deficient mutant E610A (*SI Materials and Methods*), data for mock-transfected cells are represented by open circles with thin lines. In the graphs of the other mutants, data for the WT protein and E610A mutant are represented by open squares and triangles, respectively, with thin lines. Data are means ± SD (n = 11–32). (*B*) Expression of WT and mutant CmABCB1 used for the experiments in *S. cerevisiae* AD1-8u$^-$ cells. (*C*) Rhodamine 6G concentration dependence of ATPase activity of CmABCB1 mutants. The ATPase activity was measured as a function of rhodamine 6G concentration with 5 mM ATP at 37 °C. Data are means ± SD (n = 3). Solid lines are fits of equations to the data, as described in *SI Materials and Methods* (Eq. **S1**).

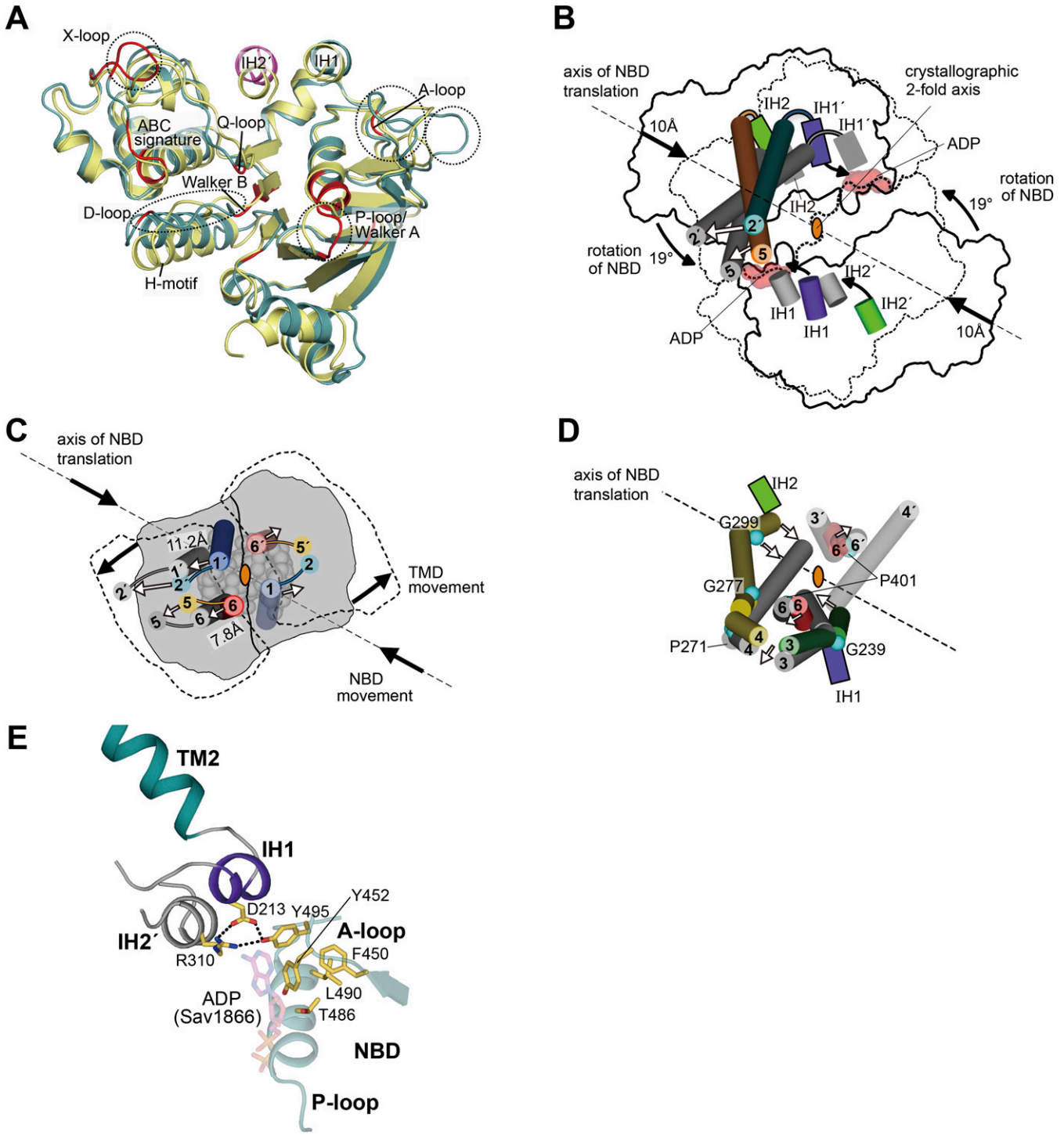

Fig. S7. Structural comparison between CmABCB1 and Sav1866 (PDB code 2HYD). (*A*) Superposition of NBD domains of CmABCB1 (light teal) and Sav1866 (pale yellow) alone, rather than as whole molecules. Significantly displaced regions are indicated by dashed circles. Representative ABC motifs of CmABCB1 are shown in red. (*B–D*) Superpositions between the dimers of CmABCB1 and Sav1866, using Cα positions, viewed from the extracellular side. The crystallographic twofold axis at the center of the CmABCB1 homodimer is depicted as ellipses. Thick arrows indicate either the rotation and translation of NBD or the motion of TM helices from the inward- to outward-facing states. In *B*, the surfaces of the NBDs of CmABCB1 and Sav1866 are depicted as solid and dashed lines, respectively. In *C*, surfaces of the TMDs of CmABCB1 and Sav1866 are depicted as solid and dashed lines, respectively. The extracellular parts of the TM helices are shown, and residues of the four-layered cluster on TM1, TM6, TM1′, and TM6′ are shown as gray spheres. In *D*, TM6 is partially represented (residues 399–403). (*E*) Conserved residues around the interface between IH1, IH2′, and the NBD of CmABCB1. ADP (translucent sticks with magenta carbon) of Sav1866 is superposed onto the NBD of CmABCB1. Conserved residues that form hydrogen bonds between IH1, IH2′, and the NBD, and those that form the nucleotide-binding site, are shown as sticks (yellow carbons).

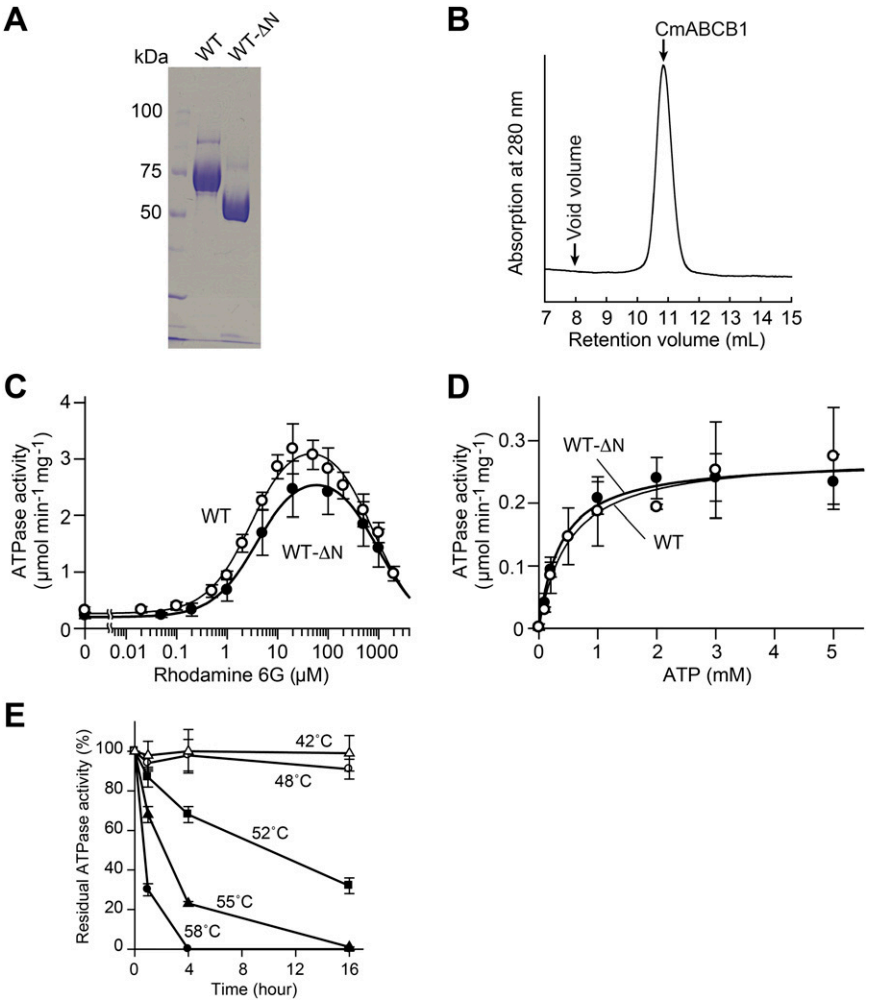

Fig. S8. Characterization of purified CmABCB1. (*A*) Coomassie-stained SDS/PAGE gel of the full-length (WT) and proteolytically N-terminally truncated (WT-ΔN) WT CmABCB1 purification products. (*B*) SEC profile of WT-ΔN on a Superdex 200 10/300 GL column. A sample of IMAC-purified WT-ΔN was loaded onto the column and eluted with 20 mM Tris·HCl (pH 7.0), 150 mM NaCl, and 0.2% (wt/vol) βDM. The arrows indicate the void volume and the elution profile of WT-ΔN, respectively. (*C* and *D*) Rhodamine 6G and ATP concentration dependence of CmABCB1 ATPase activity. The ATPase activity of WT and WT-ΔN was measured as a function of rhodamine 6G ATP concentration with 5 mM ATP (*C*) or as a function of ATP concentration (*D*) at 37 °C. Data are means ± SD ($n = 3$). Thick and thin solid lines are fits of equations to the data, as described in *SI Materials and Methods* (*C*, Eq. **S2**; *D*, Eq. **S1**). (*E*) Thermostability of CmABCB1 ATPase activity. Purified full-length CmABCB1 was preincubated in 20 mM Tris·HCl (pH 7.5), 150 mM NaCl, and 0.05% (wt/vol) βDDM for the indicated times at 42, 48, 52, 55, or 58 °C. At the indicated time intervals, aliquots were used for ATPase assays. Residual ATPase activities of the preincubated samples were calculated from the specific ATPase activity, which was determined by subtracting the basal activity from the rhodamine 6G–stimulated activity, expressed as a percentage of the original specific activity. Data are means ± SD ($n = 3$).

Table S1. Kinetic parameters of ATPase activity

	Rhodamine 6G*					ATP†	
CmABCB1	k_{basal} (s^{-1})	k_{sub} (s^{-1})	k_{sub}/k_{basal} (-fold)	K_m^{Drug} (μM)	K_i^{Drug} (μM)	k_{cat} (s^{-1})	K_m^{ATP} (mM)
WT	0.70 ± 0.17	8.9 ± 0.9 (6.3 ± 0.2)	13 ± 3 (9.0 ± 2.2)	2.9 ± 0.5 (12 ± 1)	799 ± 210 (3098 ± 87)	0.84 ± 0.18	0.60 ± 0.05
WT-ΔN‡	0.44 ± 0.07	6.2 ± 0.6	14 ± 1	3.6 ± 1.1	1077 ± 353	0.61 ± 0.12	0.40 ± 0.07
GAA/VVV§	0.13 ± 0.02	0.031 ± 0.014	0.23 ± 0.07	—	78 ± 21¶	0.13 ± 0.04	0.43 ± 0.01
F138A	1.4 ± 0.1	7.4 ± 0.7	5.2 ± 0.5	28 ± 3	1353 ± 305	1.7 ± 0.4	0.49 ± 0.07
Y358A	0.24 ± 0.07	4.0 ± 0.1	18 ± 4	57 ± 11	—	0.28 ± 0.05	0.44 ± 0.05
F384A	0.47 ± 0.01	3.4 ± 0.7	7.2 ± 1.5	20 ± 5	1856 ± 440	0.41 ± 0.05	0.55 ± 0.09
I387A	0.12 ± 0.02	2.7 ± 0.9	24 ± 12	168 ± 53	482 ± 180	0.096 ± 0.013	0.26 ± 0.06
L388A	0.97 ± 0.20	5.0 ± 1.1	5.2 ± 0.1	3.3 ± 0.3	2057 ± 128	1.4 ± 0.2	0.70 ± 0.03

Data are means ± SD (n = 3).

*ATP hydrolysis conditions were as follows: 50 mM Tris·HCl (pH 7.5), 150 mM NaCl, 0.1 mM EGTA, 0.05% (wt/vol) βDDM, 10 mM $MgCl_2$, 5 mM ATP, and various concentration of transport substrate, rhodamine 6G; reactions were performed at 37 °C. Kinetic parameters for rhodamine 6G were determined as follows: WT, WT-ΔN, F138A, F384A, I387A and L388A: Eq. **S2**; Y358A: Eq. **S3**; GAA/VVV: Eq. **S4** (*SI Materials and Methods*). k_{basal} and k_{sub} are the catalytic rate constants of ATPase activity in the absence and presence of rhodamine 6G, respectively; k_{sub}/k_{basal} is the fold stimulation by rhodamine 6G; K_m^{Drug} is the apparent Michaelis constant for rhodamine 6G with 5 mM ATP; K_i^{Drug} is the inhibition constant for substrate inhibition by rhodamine 6G. The values in parentheses are the kinetic constants for verapamil (Fig. 1*E*).

†ATP hydrolysis conditions were as follows: 50 mM Tris·HCl (pH 7.5), 150 mM NaCl, 0.1 mM EGTA, 0.05% (wt/vol) βDDM, 10 mM $MgCl_2$, and various concentrations of ATP in the absence of transport substrates at 37 °C. Kinetic parameters for ATP were determined using the Michaelis-Menten equation (Eq. **S1**) as described in *SI Materials and Methods*. k_{cat} is the catalytic rate constant of ATPase activity in the absence of transport substrates; K_m^{ATP} is the Michaelis constant for ATP in the absence of transport substrates.

‡Proteolytically N-terminally truncated WT.

§Proteolytically N-terminally truncated G277V/A278V/A279V mutant.

¶K_i value in Eq. **S4** is shown.

Table S2. Data collection

Data collection	Native (WT)	VVV mutant	VVV + peptide	Hg derivative (WT)		
Space group	*R*32	*R*32	*R*32	*R*32		
Cell dimensions						
a, *b*, *c* (Å)	180.3, 180.3, 152.3	180.5, 180.5, 156.1	180.5, 180.5, 153.2	179.8, 179.8, 159.3		
α, β, γ (°)	90, 90, 120	90, 90, 120	90, 90, 120	90, 90, 120		
			Peak	Inflection	Remote	
Wavelength	1.0000	1.0000	1.0000	1.00600	1.00906	0.99290
Resolution (Å)*	50–2.75 (2.80–2.75)	50–2.60 (2.69–2.60)	50–2.40 (2.49–2.40)	50–3.10 (3.15–3.10)	50–3.10 (3.15–3.10)	50–3.10 (3.15–3.10)
R_{sym}*	0.059 (0.371)	0.071 (0.474)	0.085 (0.575)	0.071 (0.365)	0.063 (0.354)	0.076 (0.374)
Total reflections	195,418	509,478	409,037	204,171	203,928	204,668
Unique reflections	24,596	30,069	36,663	18,055	18,031	18,117
$I/\sigma I$*	52.3 (6.7)	69.0 (6.1)	54.8 (4.8)	54.8 (8.7)	55.6 (9.2)	54.7 (8.8)
Completeness (%)*	99.3 (100)	99.8 (98.8)	98.6 (96.7)	99.8 (100.0)	99.8 (100.0)	99.8 (100.0)
Redundancy*	7.9 (6.7)	16.9 (10.6)	11.2 (9.9)	11.3 (11.4)	11.3 (11.5)	11.3 (11.5)
Phasing power				0.8	0.6	0.7
Figure of merit				0.58		
No. of sites					4	

*Highest resolution shell is shown in parentheses. $R_{sym} = \sum_h \sum_i |\langle I(h)\rangle - I_i(h)| / \sum_h \sum_i I_i(h)$, where $\langle I(h)\rangle$ is the mean intensity of equivalent reflections.

Table S3. Refinement statistics

Refinement	Native (WT)	VVV mutant	VVV + peptide
Resolution (Å)	37.8–2.75	34.9–2.60	50.0–2.40
No. reflections	24,575	29,935	35,124
R_{work}/ R_{free}*	0.209/0.275 (0.312/0.389)	0.207/0.246 (0.288/0.352)	0.208/0.242 (0.287/0.372)
No. atoms			
Protein	4,329†	4,369†	4,401‡
Detergent	23	23	91
Peptide	0	0	146
Water	20	64	123
B-factors			
Protein	88.1	86.5	62.1
Detergent	149.5	141.0	114.3
Peptide	—	—	83.0
Water	58.9	59.4	55.5
RMS deviations			
Bond lengths (Å)	0.008	0.008	0.010
Bond angles (°)	1.088	1.122	1.388
Ramachandran plot (%)§			
Favored region	95.73	96.76	96.84
Allowed region	4.10	3.07	3.16
Outlier region	0.17	0.17	0.00

*Highest resolution shell is shown in parentheses. $R_{sym} = \sum_h \sum_i |\langle I(h)\rangle - I_i(h)| / \sum_h \sum_i I_i(h)$, where $\langle I(h)\rangle$ is the mean intensity of equivalent reflections.
†Disordered regions (^{92}ASGPESAYT^{101} and ^{690}SGDMSAA^{696}) are excluded from the coordinates.
‡Disordered regions (^{92}ASGPESAYT^{101} and ^{691}GDMSAA^{696}) are excluded from the coordinates.
§As defined in MolProbity.

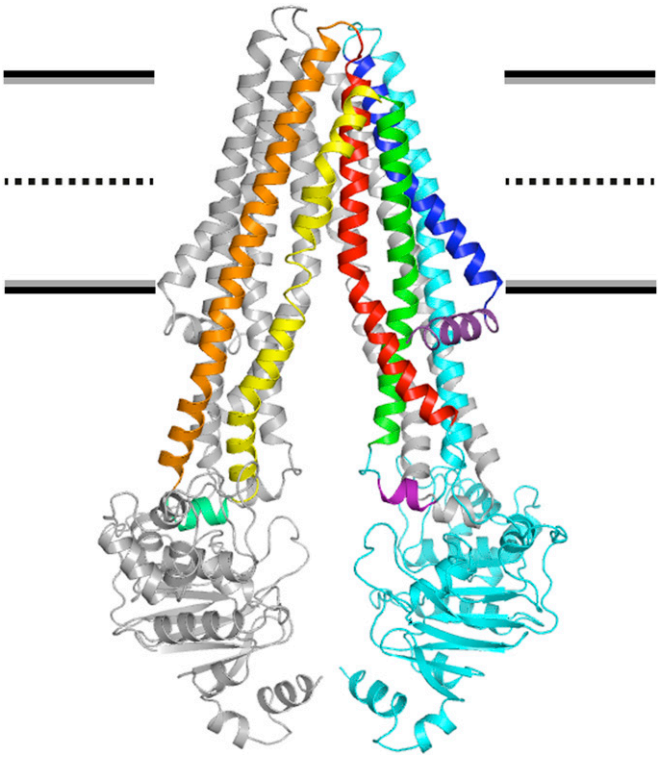

Movie S1. Structural change between inward- and outward-facing states of CmABCB1. A morph between the inward-facing CmABCB1 crystal structure and the outward-facing CmABCB1 model, based on the Sav1866 crystal structure. The outward-facing model was calculated using the automodel class of MODELER 9.11 and evaluated using DOPE potential. The structures are aligned using the superpose command of PyMOL 1.6 (1). The morphing movies of the conformational change of CmABCB1 were calculated using the morph command of PyMOL 1.6 (1).

Movie S1

1. Schrödinger L (2010) *The PyMOL Molecular Graphics System, Version 1.6* (Schrödinger, LLC, New York).